19th Australasian Fluid Mechanics Conference
Melbourne, Australia
8-11 December 2014

Numerical Simulation of the Impact of Ventral Sting on Supersonic Aerodynamics and Flow Field

LIU Xu, LIU Wei and WU Tianzuo

College of Areospace Science and Engineering
National University of Defense Technology, Changsha 410073, China

Abstract

In supersonic or hypersonic air tunnel testing, the model is generally mounted with tail support. In some special cases, however, ventral sting is used. Ventral sting does not only induce shock waves around the support, its wake also modifies the bottom flow distribution and surface pressure coefficient of the model, causing changes in the aerodynamics and flow structure across the model in the form of support interference. In this paper, the circular flow field of a blunt body under supersonic inflow with and without ventral support is simulated by solving the RANS equation with the FVM second-order accuracy Roe scheme, and the possible impact of different ventral support profiles on the aerodynamics and flow field of the model is examined through comparison of the aerodynamics and pressure distribution under different conditions, together with characterization of the flow structure of the model. The result shows that ventral sting has considerable impact on the aerodynamics of the model; different ventral support profiles vary in their amount of interference; and the presence of ventral sting modifies the pressure distribution at the bottom of the model. It is recommended that ventral sting be designed to avoid the induction of detached shock waves and the effect of a significant separated region on the model.

Introduction

In supersonic air tunnel testing, the model is generally mounted with tail support. Previous studies on support interference has mostly been made under subsonic or transonic conditions [1-7], with the latter having received a range of experiments and calculations. It is generally accepted that tail support is not as influential on model aerodynamics as ventral support. For specific experiments like those in connection with the characterization of rocket nozzles, the bottom flow of rocket boosters or stage separation of missiles where ventral support is but the only choice, it is also highly necessary to examine the impact of ventral support on the aerodynamics and bottom flow of the model.

In this paper, the circular flow field of a blunt tricone with and without support is numerically simulated by dividing the flow field with a structured patched grid, using FVM for the RANS equation, a 2-order accuracy Roe scheme for spatial discretion and LU-SGS method for time solution; The impact of different ventral support profiles on the aerodynamics and flow field of the model is examined by comparing the aerodynamics and pressure distribution under different conditions together with characterization of the flow structures.

Computational Models and Grid

The computational models used are an unsupported spherical tricone and a tricone with ventral support. The latter consists of the spherical tricone and a ventral support (figure 1) with the following parameters: Head radius: 3.35; total length: 154.67; cone angles: 17º20′, 10º50′, 4º; cone bottom diameters: 30.85, 36.10, 50; vertical distance from the front of the support-model intersection to the vertex of the head: 79.76. The calculation used the total length the reference length, the cone bottom area as the reference area and the vertex of the head as the moment reference point. Structured computational grids for the profiles were generated taking into account the characteristics of a physical model, the practical workload and computational conditions. The grid for the profile with ventral support contained ca. 4.7 million cells. The first layer of cells for the head is 1×10^{-4} apart from the object plane so as to maintain the dimensionless scale of $y^+<1$. The grid for the symmetrical plane is as shown in figure 2. A total of 8 blocks were used with no singular axis. The grid was generated at the support that enveloped the entire support. The grid for the unsupported model contained ca. 1.243 million cells with singular axis at the head and tail. Figure 3 shows the grid for the symmetrical plane and the surface.

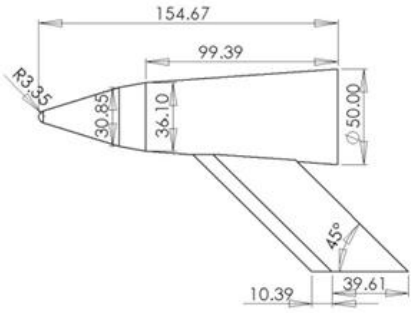

Figure 1. Outside dimensions of the spherical tricone with ventral support

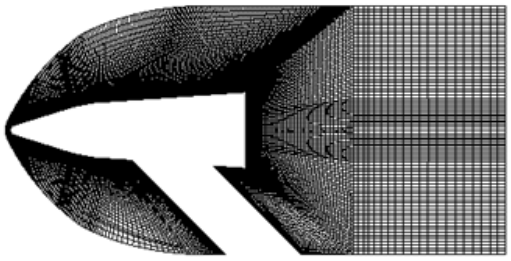

Figure 2. Grid for symmetrical plane with support

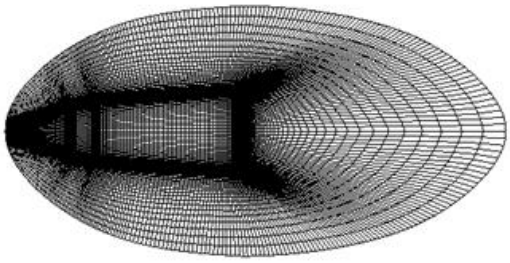

Figure 3. Grid for symmetrical plane and surface without support

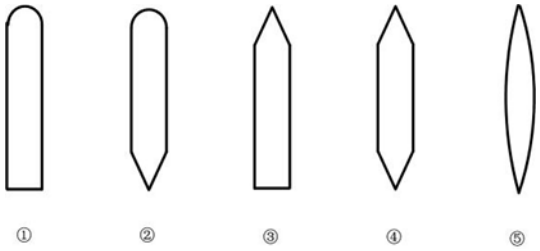

Figure 4. Cross-sectional shape of the support

To examine the impact of different shapes of support on the model aerodynamics, 5 support profiles were designed as shown in figure 4. Profiles ①-⑤ are identical in length and wide, mounted at the same position of the model and with the same sweepback. Profile ③ is the base support profile. The base support is 12 thick with leading-edge apex angle of 30°. The entire support sweepback is 45°. The longitudinal length is 50. Main differences among the supports are the shapes of the leading and trailing edges. The leading edges of profiles ①② are semicircular. That of profile ⑤ is a symmetrical one consisting of two cambered surfaces.

Numerical Algorithm

Numerical calculation included the use of FVM to solve the RANS equation, a two-order accuracy Roe scheme to discretize spatial terms, LU-SGS to solve temporal terms and SA model as the turbulence model. Calculation was carried out assuming that air was an ideal gas, the free inflow Mach number was 3.26, the inflow temperature was 150K and the Reynolds number based on reference length was 10.15×10^6.

In an air tunnel testing, the two-step method may be used for the purpose of interference correction, and the interference quantity is derived from the difference between the calculated aerodynamic forces with and without a mirror support. In our numerical calculation, an approach similar to the two-step method was used and the interference quantity was established from the difference between the calculated aerodynamic forces with and without a support.

Calculation Results

Table 1 presents the aerodynamic forces with and without a ventral support, calculated with a turbulence SA model. Tables 2-4 list the aerodynamic figures under different support profiles, calculated at the attack angle of 0°, 10° and -10°. As can be observed from data shown in these tables, the presence of a support is significant on all the aerodynamic parameters of the model. Figures 5-7 compare the support interference quantities under different support profiles.

angle of attack	Cm	Cn	Ca
-10	-0.2208	-0.4245	0.2580
0	0.0000	0.0000	0.1243
10	0.2208	0.4245	0.2580

Table 1. Calculation result without a support

	Cm	Cn	Ca
support1	-0.0039	0.0014	0.2487
support2	-0.0011	0.0050	0.2490
support3	-0.0047	0.0001	0.2486
support4	-0.0073	-0.0031	0.2484
support5	-0.0038	0.0001	0.2488

Table 2. Comparison model aerodynamics at attack angle of 0° under support of different cross sections

	Cm	Cn	Ca
support1	0.1797	0.3799	0.3229
support2	0.1825	0.3836	0.3240
support3	0.1822	0.3826	0.3233
support4	0.1815	0.3813	0.3235
support5	0.1923	0.3941	0.3264

Table 3. Comparison model aerodynamics at the attack angle of 10° under support of different cross sections

	Cm	Cn	Ca
support1	-0.2061	-0.4000	0.3296
support2	-0.2053	-0.3987	0.3298
support3	-0.2066	-0.4015	0.3298
support4	-0.2095	-0.4050	0.3305
support5	-0.2108	-0.4077	0.3309

Table 4. Comparison model aerodynamics at the attack angle of -10° under support of different cross sections

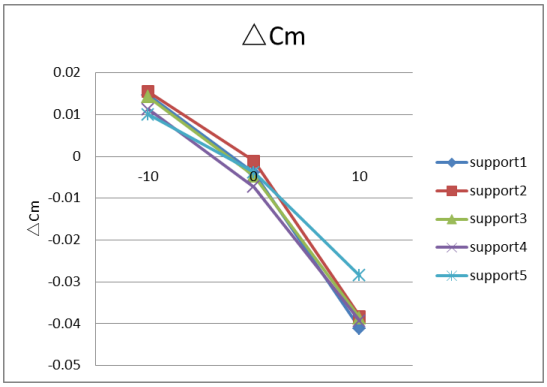

Figure 5. △Cm variation with attack angle

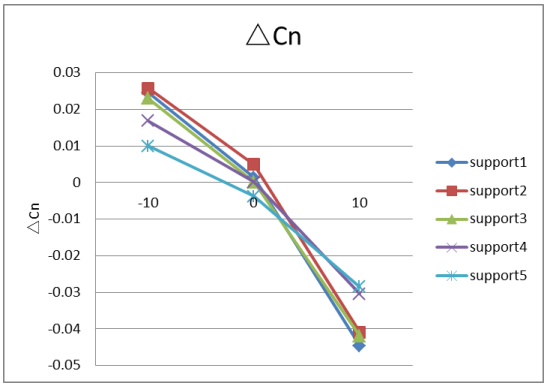

Figure 6. △Cn variation with attack angle

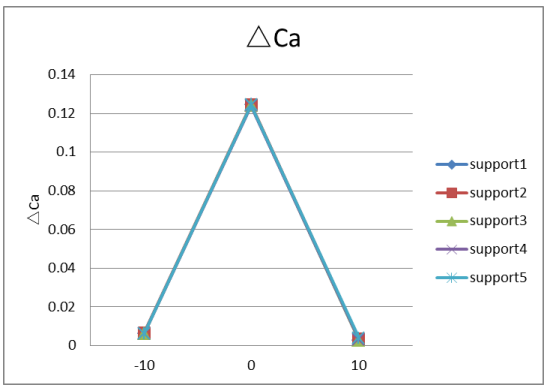

Figure 7. △Ca variation with attack angle

At large, different support profiles tend to have roughly the same impact on the model aerodynamics, except that greater impact is observed when the attack angle is positive than when it is negative. The shape of the support leading edge typically acts on the relative position of the support front shock, and sharp leading edge induces attached shock at the support leading edge, thereby resulting in different flow structures at this position which in turn gives rise to divergent aerodynamic forces. The profile of the trailing edge, on the other side, constrains the support wake region. As a sharp trail edge does not induce a large flow separated region, it's not so influential on the flow when support is provided.

Relative to the pitching moment coefficient, at any attack angle other than 0 °, support ⑤ has the least interference and supports ①③ are more influential. This suggests that a horizontal cross-sectioned trailing edge is more influential on the pitching moment; at the attack angle of 0 °, support ② has the least interference.

Relative to the normal force coefficient, the sharp-headed sharp-tailed supports ④⑤ show limited influence at any attack angle; supports ①②③ are quite the same, and the blunt-headed leading edge supports ①② show greater interference.

Relative to the axial force coefficient, the interference to the support is greater at the attack angle of 0 ° and modest at any other attack angle. The support profiles do not show much difference in the axial force coefficient at any other than 0 °.

Generally speaking, the minimal support interference with good regularity is the goal for any aerodynamic designer. As can be concluded from the support interference curves shown above, support ⑤ has the least interference. It is therefore an ideal choice for static experiment of the model.

Figure 8 shows the pressure distribution on the model surface and symmetrical plane at attack angle of 0 ° without support and under different support profiles. As can be seen from figure 8(b)-(f), the pressure distribution on the upper half of the model is roughly the same under different support profiles; the ventral support typically acts on the flow distribution on the lower half of the model and does not have much influence on the flow field of either the upper half of the model or of the model when no support is provided. This is because, under supersonic inflow, the flow field does not propagate backward when it is interfered but only acts over a modest distance at the support leading edge, while significant change can be expected in the flow field when support is provided due to the presence of this support.

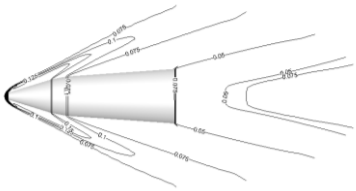

Figure 8.(a) Without support

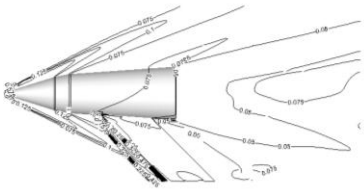

Figure 8.(b) Support ①

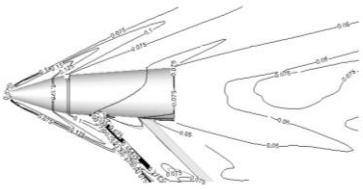

Figure 8.(c) Support ②

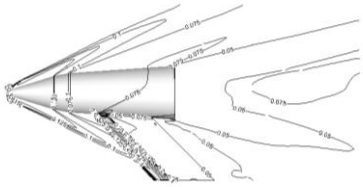

Figure 8.(d) Support ③

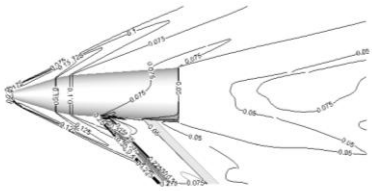

Figure 8.(e) Support ④

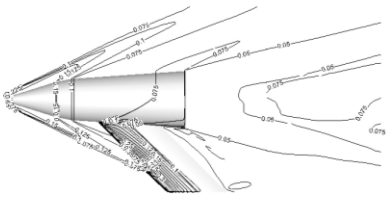

Figure 8.(f) Support ⑤

Figure 8. Pressure distribution on surfaces and symmetrical planes at attack angle of 0 °without support and under different support profiles

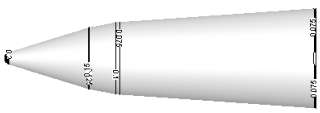

Figure 9.(a) Without support

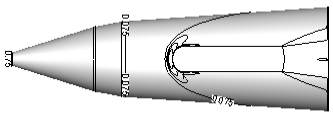

Figure 9.(b) Support ①

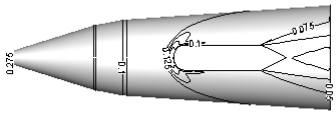

Figure 9.(c) Support ②

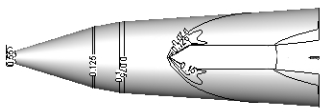

Figure 9.(d) Support ③

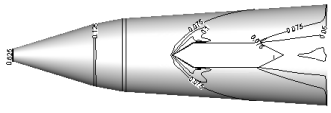

Figure 9.(e) Support ④

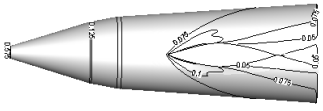

Figure 9.(f) Support ⑤

Figure 9. Lower surface pressure distribution at attack angle of 0 °without support and under different support profiles

Figure 9 shows the lower surface pressure distribution of the model at attack angle of 0° under different support profiles Supports ①② and ③④ have the same leading edge profile but are different in the trailing edge. It can be observed that their pressures are roughly the same at the support leading edge but vary significantly at the trailing edge. Expansion shock occurred at the trailing edge. The different positions at which expansion shock occurred accounted for the different surface pressure distributions and thereby the aerodynamic distribution of the model. Supports ①③ and ②④ have the same trailing edge profile but are different in leading edge. It can be observed that their pressures are roughly the same at the support trailing edge but vary significantly at the leading edge. This is explained by the different shock shapes: a sharp leading edge will produce attached shock while a blunt one will produce detached shock at the support leading edge, which in turn expands the area of influence of the support. From figure 9(f), a smoother profile acts more smoothly on the flow field, and a sharp leading edge produces attach shock which, compared with ③④, does not result in heavy separation at a point where the support varies violently and is thereby less influential on the flow field.

Figure 10 shows the bottom pressure distribution of the model without support. Figures 11 and 12 show the bottom pressure distribution of the model under typical supports ③ and ⑤. Presence of a ventral support accounted for changes in the pressure at the center of the model bottom: the pressure contour nearer the support is denser, which changed the pressure distribution at the model bottom.

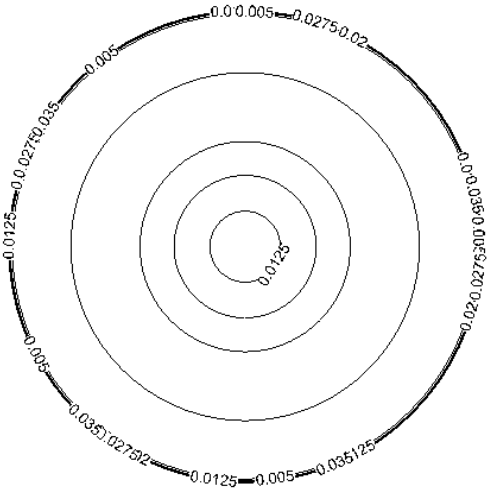

Figure 10. Bottom pressure distribution without support

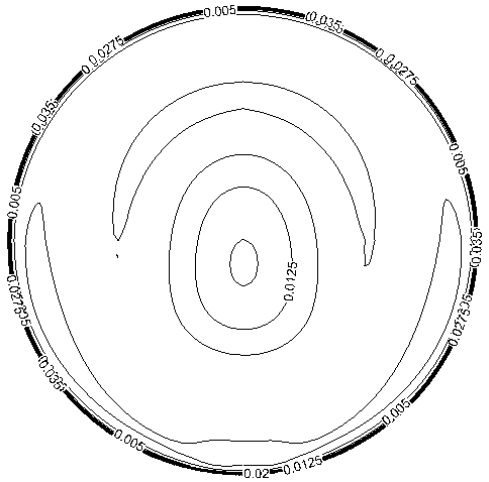

Figure 11. Bottom pressure distribution under support ③

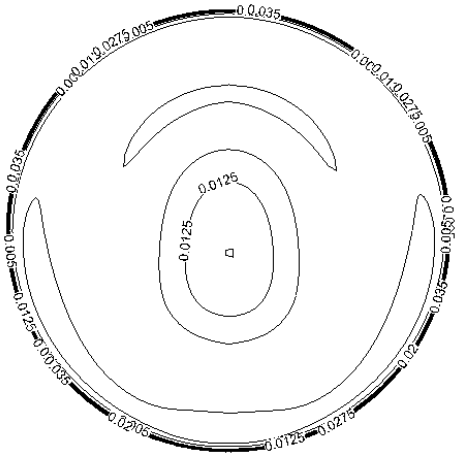

Figure 12. Bottom pressure distribution under support ⑤

Conclusions

Numerical simulation of the flow field of the model with ventral support of different cross-sectional shapes is carried out under supersonic inflow, from which the following conclusions are made:

Ventral support has significant impact on the aerodynamics of the model. Ventral supports of different shapes vary in their interference quantity. It is demonstrated that a double-camber symmetrical support has the least support interference; ventral supports of different profiles show greater interference when the attack angle is positive than when it is negative; ventral support should be designed to avoid the induction of detached shock and the impact of a sizable separated region on the model; presence of ventral support modifies the pressure distribution at the model bottom.

References

[1] Blaha, B.J. & Lewis Research Center., Wind tunnel blockage and support interference effects on winged-body models at Mach numbers from 0.6 to 1.0. *NASA technical memorandum.* 1974.

[2] Compton, W.B. & United States. National Aeronautics and Space Administration., Jet exhaust and support interference effects on the transonic aerodynamic characteristics of a fighter model with two widely spaced engines. *NASA technical memorandum*. 1976.

[3] Ericsson, L. & J. Reding, Review of support interference in dynamic tests. *AIAA journal*, 1983. 21(12): p. 1652-1666.

[4] Loving, D.L., Sting-support interference on longitudinal aerodynamic characteristics of cargo-type airplane models at Mach 0.70 to 0.84. *NASA technical note.* 1967.

[5] Taylor, G. & I. Gursul, Support interference for a maneuvering delta wing. *Journal of aircraft*, 2005. 42(6): p. 1504-1515.

[6] Tuttle, M.H. & P.L. Lawing, National Aeronautics and Space Administration. Scientific and Technical Information Branch., Support interference of wind tunnel models : a selective annotated bibliography. *NASA technical memorandum.* 1984.

[7] Vlajinac, M., Massachusetts Institute of Technology., and Langley Research Center., Subsonic and supersonic static aerodynamic characteristics of a family of bulbous base cones measured with a magnetic suspension and balance system. *NASA contractor report.* 1972.